

Electronic, Optical and Elastic Properties of Perovskite $\text{CsSnI}_{3-x}\text{Cl}_x$ ($x = 0, 1, 2, 3$): Using First Principles Study

Amondulloi S. Burkhonzoda ^{1,*}, Dilshod D. Nematov ^{1,*}, Mekhrdod S. Kurboniyon ^{1,2}, Umar Zafari ^{1,3},
Kholmurzo T. Kholmurodov ^{1,6,7}, Tomoyuki Yamamoto ^{4,5}, Farhod Shokir ¹

¹ S.U. Umarov Physical-Technical Institute of the NAST, Dushanbe 734063, Tajikistan

² School of Optoelectronic Engineering & CQUPT-BUL Innovation Institute, Chongqing University of
Posts and Telecommunications, Chongqing, 400065, China

³ Center of Innovative Development of Science and New Technologies, NAST, Dushanbe, 734025, Tajikistan

⁴ Faculty of Science and Engineering, Waseda University, Tokyo, 169-8555, Japan

⁵ Institute of Condensed-Matter Science, Waseda University, Tokyo, 169-8555, Japan

⁶ Joint Institute for Nuclear Research, 141980 Dubna, Russia

⁷ Dubna State University, 141980 Dubna, Russia

* Correspondence: dilnem@mail.ru, amondullo.burkhonzoda@mail.ru

Abstract. The structural, electronic, optical and elastic properties of perovskites of the α -, β - and γ -phase family $\text{CsSnI}_{3-x}\text{Cl}_x$ ($x = 0, 1, 2, 3$) are analyzed by ab initio methods using GGA, SCAN and HSE06. It is found that the lattice constants of $\text{CsSnI}_{3-x}\text{Cl}_x$ decrease with decreasing anion size from I to Cl, and when passing from CsSnI_3 to CsSnCl_3 , the band gap width decreases slightly at the beginning and then increases. The optical characteristics were evaluated and it was found that the α -, β -phase of $\text{CsSnI}_{3-x}\text{Cl}_x$ at $x=1$ has a wide absorption range and high absorption coefficients compared to other Cl concentrations. The elastic constants of α - $\text{CsSnI}_{3-x}\text{Cl}_x$ perovskite have been calculated and their bulk moduli, shear moduli, sound velocities and Debye temperatures under pressure in the range from 0 to 30 GPa have been considered, with the external pressure induction increasing in steps of 5 GPa. These materials are found to be mechanically stable perovskites according to Born stability criteria and low bulk moduli. Thus, we predict that perovskites of the $\text{CsSnI}_{3-x}\text{Cl}_x$ family are good candidates for optical materials used in solar cells.

Keywords: lead-free perovskites, electronic and optical properties, elastic modules, band gap, DFT, photovoltaic applications, solar cells.

1. Introduction

Due to population growth and the resulting increase in the need for electrical energy, the last decade has seen the search for high-efficiency materials to create and develop solar cells by various methods [1-3]. The most common material capable of absorbing sunlight and converting it into electrical energy is silicon. In principle, silicon is the basis for most modern single junction solar cells. However, silicon does not have an easily tunable band gap and is not suitable for photovoltaic or multi-junction solar cells, and has a number of limitations and low efficiency.

As a result of numerous experimental studies and theoretical calculations, some photovoltaic materials such as copper-indium-gallium selenide (CIGS), cadmium telluride (CdTe) and iron disulfide (FeS_2) have been found and studied, which have much higher efficiency compared to silicon [10-16]. In addition, much higher efficiencies can be achieved with multilayer cells made of other semiconductor materials. For example, the efficiency of solar cells made of AlGaInP , AlGaAs , GaAs is 47.1% [25]. However, all these compounds are expensive due to the presence of scarce elements, and their production on an industrial scale cannot be realized yet.

Meanwhile, perovskite crystals have attracted much research attention due to their important chemical, electronic, mechanical and photovoltaic properties such as high absorption capacity, high carrier mobility, low exciton binding energy and attractiveness for use in solar cells [4-9]. Metal halide perovskites having the form ABX_3 (here $\text{A} = \text{Cs}, \text{Rb}, \text{MA} (\text{CH}_3\text{NH}_3^+)$, $\text{FA} (\text{CH}_2(\text{NH}_2)^{2+})$; $\text{B} = \text{Pb}^{2+}, \text{Ge}^{2+}$; $\text{X} = \text{I}, \text{Br}^-, \text{Cl}^-$ or mixed X- anions) show great potential for solar

cell applications due to their excellent absorption coefficient, long lifetime and easily controlled band gap [17-25]. Among these compounds, the use of lead halide perovskites (CsPbX_3) as absorbers in solar cells has several advantages and disadvantages over other halide perovskites. Their small band gap and good absorption capacity make them a good material for optoelectronic applications, but these structures are unstable at ambient temperature, which hinders their practical use [28-29] and commercialization [30]. However, one of the major disadvantages of Pb is that Pb^{2+} is toxic and Pb-based perovskites pose serious health and environmental hazards. Despite the breakthrough of 26.1% (USTC) energy conversion efficiency demonstrated in organic-inorganic hybrid perovskite solar cells [26-27], there are still critical issues related to instability and toxicity that could potentially hinder their commercialization.

Therefore, replacement of lead by other non-toxic elements is highly desirable. Recent review articles [35-37] emphasized the need to develop new perovskite materials with a direct band gap and outlined the scientific problems associated with lead-free perovskites. Thus, to obtain lead-free material for photovoltaic applications, the B site in ABX_3 ($\text{B} = \text{Pb}^{2+}$) can be replaced by other divalent metals such as Sr^{2+} , Ge^{2+} , Zn^{2+} , Sn^{2+} [31-34]. The most suitable substitution for the Pb position is the divalent metal Sn because Sn and Pb belong to group 14 of Mendeleev's periodic table and hence have similar physicochemical properties [38-40].

Understanding the structural, electron-optical and mechanical properties of these materials for use in α -, β - and γ -phase $\text{CsSnI}_{3-x}\text{Cl}_x$ hybrid solar cells is highly desirable, which is investigated in this work.

2. Computational methods

The calculations were performed using the Vienna ab initio simulation package (VASP) [41] in the framework of density functional theory (DFT). At the first stage of the study, a thorough convergence check on the cutoff and KPOINTS energies was carried out, resulting in their optimal values for further calculations.

Thus, a value of 500 eV was chosen as the cutoff energy for all $\text{CsSnI}^{3-x}\text{Cl}^x$ phases. The Monkhorst-Pack k-point grid sampling was set to $4 \times 4 \times 4$, $5 \times 5 \times 7$, and $3 \times 3 \times 2$ for α - (cubic Pm-3m (221)), β - (tetragonal P4/mbm (127)), and γ - (rhombohedral Pnam (62)) phases, respectively. All crystals were optimized using the same software and under the same conditions. The generalized gradient approximation proposed by Perdew, Burke, and Ernzerhof (GGA-PBE) [42] was used to express the electron-electron correlation, while the more accurate meta-GGA (SCAN) [43] and hybrid (HSE06) [44] functionals were used to calculate the electronic properties, since GGA usually underestimates the band gap magnitude for these compounds.

The elastic properties were calculated under the same conditions using the GGA-PBE approximation. The k-point value of the Monkhorst-Pack k-point grid was doubled to calculate the DOS. The optical properties of $\text{CsSnI}_{3-x}\text{Cl}_x$ were calculated from the SCAN-optimized structure using the GGA [57] -mBJ [58] potentials implemented in the WIEN2K package [59] with $10 \times 10 \times 10$ k-point Brillouin zone.

Machine learning models [72] can give a general idea of the expected value of the bandgap for inorganic and halide perovskites. A linear regression model using Python code was used to predict the band gap of α -, β -, and γ -phases of $\text{CsSnI}_{3-x}\text{Cl}_x$ [62].

3. Results and discussion

3.1. Structural properties

$\text{CsSnI}_{3-x}\text{Cl}_x$ ($x = 0, 1, 2, 3$) perovskites exist in different phases and in the present studies we focus only on α -, β -, γ - phases using DFT method, which respectively contain 5, 10, 20 atoms in the elemental cell. Figure 1(a), (b), (c) shows the optimized crystal structures of α -, β -, γ - phases of CsSnI_3 , respectively.

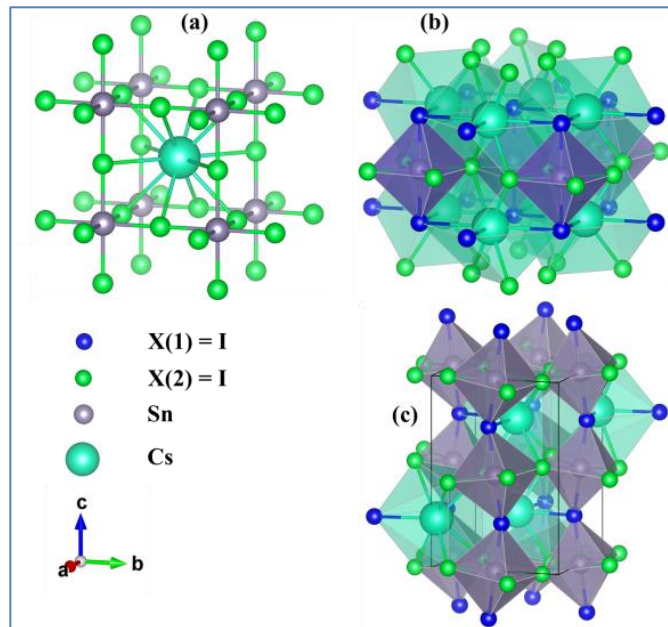


Figure 1. Crystal structures of (a) α -, (b) β -, (c) γ - phases of CsSnI_3

As can be seen from Figure 1, the β -, γ - phases of CsSnI_3 have 2 types of atom I, and site occupation was carried out to obtain the mixed structures. It is found that the I(1) position is more energetically favorable for Cl ions in CsSnI_3 .

Thus, the I atom in the α -, β -, γ - phases of the CsSnI_3 structure was replaced by Cl atoms, which were then optimized perovskite structures CsSnI_2Cl , CsSnICl_2 and CsSnCl_3 . The obtained lattice constants are shown in Table 1 and the obtained values were in a great agreement with other theoretical and experimental values. We find that the lattice constants of $\text{CsSnI}_{3-x}\text{Cl}_x$ decrease with decreasing the size of anions from I to Cl.

For optoelectronic materials, it is important to guarantee the structural and thermodynamic stability of perovskite $\text{CsSnI}_{3-x}\text{Cl}_x$ compounds, which can be evaluated using the Goldschmidt tolerance factor and octahedral factor, according to equations (1) and (2), respectively [60-61].

$$t_G = \frac{R_A + R_X}{\sqrt{2} (R_B + R_X)}, \quad (1)$$

$$\mu = \frac{R_B}{R_A}, \quad (2)$$

where R_A and R_B are the effective radius of Cs^+ and Sn^{2+} , respectively, R_X is the effective radius of the I, Cl⁻ and their average value.

The stable three-dimensional structure of halide perovskite is usually formed at $0.80 \leq t_G \leq 1.0$ and $0.44 \leq \mu \leq 0.9$. For $\text{CsSnI}_{3-x}\text{Cl}_x$, $\mu = 0.61$ and t_G values are in the range of (0.849 - 0.869), indicating a stable perovskite structure.

Table 1. Calculated lattice parameters of CsSnI_{3-x}Cl_x (x = 0, 1, 2, 3) in Å

System		This work		Other works
		GGA	SCAN	
CsSnI ₃	α (a=b=c)	6.261	6.179	6.22 [45,46]; 6.231 [49]; 6.143 [50]; 6.219 [51]; 6.28 [54]; 6.22 [56]
	β (a=b,c)	8.789, 6.318	8.680, 6.239	8.772, 6.261 [45];
	γ (a,b,c)	8.957, 8.667, 12.503	8.847, 8.533, 12.372	8.688, 8.643, 12.378 [45];
CsSnI ₂ Cl	α (a=b=c)	6.306	6.208	-
	β (a=b,c)	8.367, 6.319	8.270, 6.225	-
	γ (a,b,c)	8.327, 8.327, 12.592	8.220, 8.220, 12.394	-
CsSnICl ₂	α (a=b=c)	6.291	6.167	-
	β (a=b,c)	8.467, 5.631	7.779, 6.195	-
	γ (a,b,c)	7.884, 7.884, 12.604	7.771, 7.772, 12.385	-
CsSnCl ₃	α (a=b=c)	5.617	5.538	5.56 [46]; 5.604 [52]; 5.618, 5.615 [53]; 5.60 [55]; 5.61 [54];
	β (a=b,c)	7.898, 5.654	7.792, 5.583	-
	γ (a,b,c)	7.956, 7.884, 11.236	7.840, 7.778, 11.088	-

3.2. Electronic properties

The electronic properties of the CsSnI_{3-x}Cl_x are calculated by using GGA, SCAN and HSE06. The HSE06 functional is the most appropriate for the evaluation of the band structure and estimate band gaps comparable with the experiment. So, this functional is highly reliable for studying the electronic properties of perovskite-like systems, in comparison with GGA, which greatly underestimates the band gap. Therefore, to understand the electronic conductivity of the CsSnI_{3-x}Cl_x system (x = 0, 1, 2, 3), this paper considers the band gap magnitude, total density of states (TDOS) and partial density of states (PDOS) obtained by calculating the hybrid functional HSE06.

Table 2 summarizes the calculated band gap values and compares them with experimental and other theoretical data. The good agreement of the results for pure perovskites confirms the predicted values of the band gap of other phases of pure and mixed systems. The variation of the band gap width of α -, β - and γ - CsSnI_{3-x}Cl_x (x = 0, 1, 2, 3) is presented in Figure 2, where it can be seen that the band gap first slightly decreases and then increases when going from CsSnI₃ to CsSnCl₃. This trend in all investigated CsSnI_{3-x}Cl_x phases propagates in a similar way. This is due to the fact that the I atom has a larger size than the Cl atom. The gradual substitution of the I atom with Cl atoms leads to a decrease in the atom size and further increases the separation between the conduction band (CB) and valence band (VB).

To evaluate the material in terms of photovoltaic applications, the value of the band gap should be in the range from 1.0 to 1.5 eV. As suggested by Shockley and Kweisser, the maximum efficiency in this interval can be achieved at a band gap width of 1.34 eV [63-64]. From this point of view, according to calculations based on the hybrid potential of HSE06, all investigated

structures are good and potential materials for photovoltaic applications, except for CsSnCl_3 , whose band gap exceeds the effective limit.

Table 2. Calculated and experimental band gap of α -, β - and γ - $\text{CsSnI}_{3-x}\text{Cl}_x$ ($x = 0, 1, 2, 3$) in eV

System		This work				Exp.
		GGA	SCAN	HSE06	ML	
CsSnI_3	α	1.115	1.122	1.326	1.232	-
	β	0.942	1.108	1.230	0.876	-
	γ	1.161	1.146	1.435	1.171	1.3[48]
CsSnI_2Cl	α	1.093	1.074	1.331	1.391	-
	β	0.592	0.538	0.834	1.063	-
	γ	0.791	0.708	1.036	1.294	-
CsSnICl_2	α	1.202	1.207	1.482	1.564	-
	β	0.658	0.581	0.919	1.156	-
	γ	1.062	0.985	1.379	1.511	-
CsSnCl_3	α	1.520	1.585	1.845	1.745	1.9[47]
	β	1.359	1.472	1.758	1.360	-
	γ	1.646	1.718	2.026	1.707	-

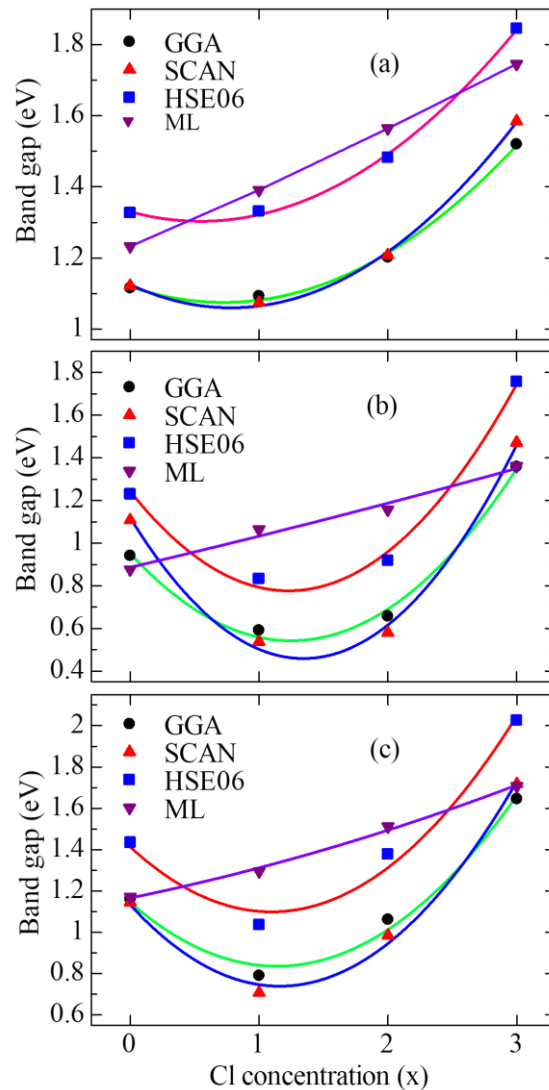


Figure 2. Calculated band gap of (a)- α -, (b)- β and (c)- γ phases $\text{CsSnI}_{3-x}\text{Cl}_x$ as function of Cl concentration x (0, 1, 2, 3), with GGA, SCAN, HSE06 functionals and ML

The total and partial densities of states of α -, β -, and γ -phases of $\text{CsSnI}_{3-x}\text{Cl}_x$ ($x = 0, 1, 2, 3$) are shown in Figures 3 and 4, respectively. The valence band maximum is zero and the dashed lines indicate the Fermi level. It can be seen from the presented figures that none of the studied structures crosses the Fermi level, and this confirms that these materials exhibit semiconducting properties. In the valence band and conduction band, the γ -phase of $\text{CsSnI}_{3-x}\text{Cl}_x$ has a large number of energy levels in the unit energy range, followed by β - and α -phases, respectively.

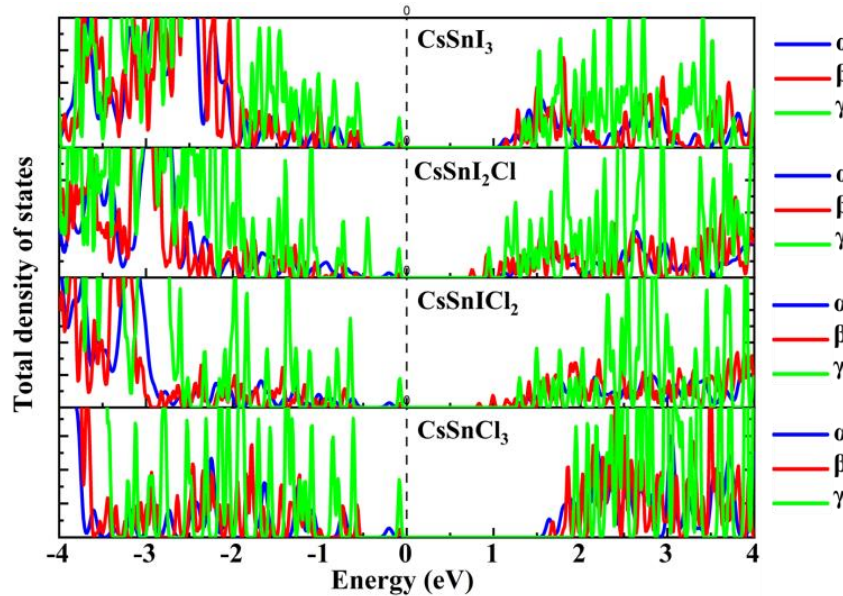


Figure 3. Total densities of states of α -, β -, and γ -phases of $\text{CsSnI}_{3-x}\text{Cl}_x$ calculated from the HSE06 hybrid functional

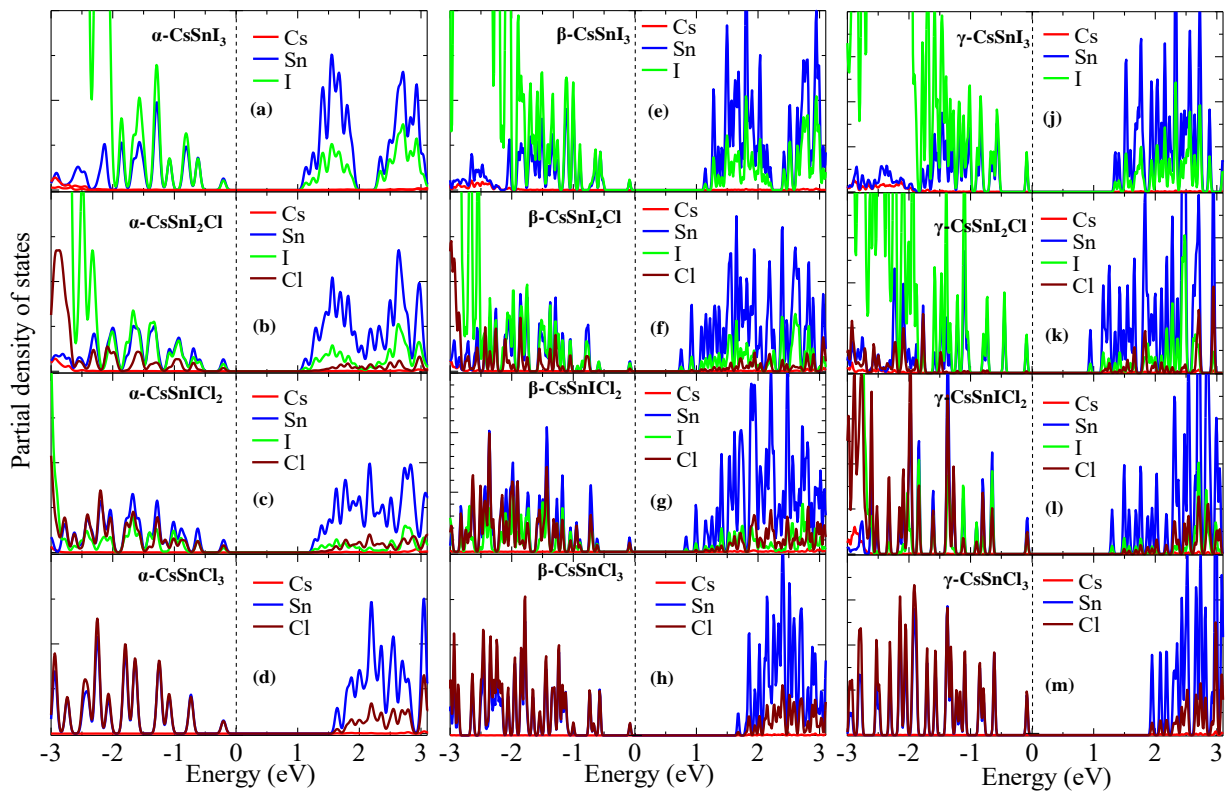


Figure 4. Partial densities of state of α -, β - and γ -phases of $\text{CsSnI}_{3-x}\text{Cl}_x$ calculated from the hybrid functional HSE06

The partial densities of electronic states (Figure 4) show the contribution of individual atoms of α -, β -, and γ -phases of $\text{CsSnI}_{3-x}\text{Cl}_x$ ($x = 0, 1, 2, 3$). In all systems, the contribution of electrons of the Cs atom is very little noticeable in the formation of the valence band (left part of the Fermi level) and conduction band (right part of the Fermi level). It can be said that the Cs atom practically does not participate in the formation of energy bands. The PDOS picture shows that the main contribution to the formation of the valence band and conduction band is made by Sn atoms and halogens, which play an important role in the appearance of the band gap. In the formation of the valence band of the α -, β - and γ -phases of CsSnI_3 , the main contribution is made by the electrons of atom I, and the contribution of the electrons of atom Sn is much smaller than that of atom I. In the conduction band formation, on the contrary, the contribution of Sn atom electrons is larger than that of I atom electrons. This tendency similarly extends to the other investigated systems. In the transition from I to Cl in the formation of the valence band and conduction band, the contribution of electrons of Cl atoms increases and plays a major role in the increase of the band gap. In contrast to other systems, the electrons of Sn and Cl atoms have almost equal shares in the formation of the valence band of α -, β -, and γ -phases of CsSnCl_3 .

3.3. Optical properties

Optical functions and optical characteristics of materials are crucial parameters to better understand the electronic configuration of materials and to determine their suitability for photovoltaic applications, since they provide important information about its interaction with light. Therefore, the study of optical properties of these halide perovskites is very important and their complex dielectric function $\varepsilon(\omega) = \varepsilon_1(\omega) + i\varepsilon_2(\omega)$ plays a fundamental role in all optical property parameters. Here $\varepsilon_1(\omega)$ and $\varepsilon_2(\omega)$ represent the real and imaginary parts of the dielectric function, respectively. Using $\varepsilon_1(\omega)$ and $\varepsilon_2(\omega)$ other parameters such as absorption coefficient $\alpha(\omega)$, reflectivity $R(\omega)$, refractive index $n(\omega)$, extinction coefficient $k(\omega)$, optical conductivity $\sigma(\omega)$ and energy loss function $L(\omega)$ can be obtained [65-68]:

$$\alpha(\omega) = \sqrt{2\omega} \left[\sqrt{\varepsilon_1^2(\omega) + \varepsilon_2^2(\omega)} - \varepsilon_1(\omega) \right]^{1/2}, \quad (3)$$

$$R(\omega) = \left| \frac{\sqrt{\varepsilon_1(\omega) + i\varepsilon_2(\omega)} - 1}{\sqrt{\varepsilon_1(\omega) + i\varepsilon_2(\omega)} + 1} \right|^2 = \frac{(n-1)^2 + k^2}{(n+1)^2 + k^2}, \quad (4)$$

$$n(\omega) = \left[\sqrt{\varepsilon_1^2(\omega) + \varepsilon_2^2(\omega)} + \varepsilon_1(\omega) \right]^{1/2} / \sqrt{2}, \quad (5)$$

$$L(\omega) = \frac{\varepsilon_2(\omega)}{\varepsilon_1^2(\omega) + \varepsilon_2^2(\omega)}, \quad (6)$$

$$k(\omega) = \left[\frac{\sqrt{\varepsilon_1^2(\omega) + \varepsilon_2^2(\omega)} - \varepsilon_1(\omega)}{2} \right]^{1/2}, \quad (7)$$

$$\sigma(\omega) = \frac{i(\omega)}{4\pi} \varepsilon(\omega). \quad (8)$$

The calculated real and imaginary parts of the dielectric functions of α -, β - and γ -phases of $\text{CsSnI}_{3-x}\text{Cl}_x$ ($x = 0, 1, 2, 3$) are plotted in the range of 0-14 eV (Figure 5). $\varepsilon_1(\omega)$ represents the stored energy of the medium or material that can be given up. $\varepsilon_2(\omega)$ explains the absorption capacity and behavior of these materials for photovoltaics. As can be seen from Figures 5(a),(b),(c), the static permeability $\varepsilon_1(0)$ is determined by the lower energy limit $\varepsilon_1(\omega)$. The $\varepsilon_1(\omega)$ peaks shift toward higher energies in the transition from I to Cl. The calculated values of $\varepsilon_1(0)$ for α -, β - and γ -phases of $\text{CsSnI}_{3-x}\text{Cl}_x$ ($x = 0, 1, 2, 3$) using the GGA-mBJ potential are summarized

in Table 3. $\epsilon_1(0)$ and the band gap are in inverse dependence on each other. Figure 9 (a) shows that $\epsilon_1(\omega)$ for the cubic phase of CsSnI₃, CsSnI₂Cl, CsSnICl₂ and CsSnCl₃ increases and reaches its maximum value of 7.71, 8.24, 4.49 and 4.65 at 1.4, 0.8, 1.51 and 1.64 eV, respectively. Figure 9 (b) shows that $\epsilon_1(\omega)$ for the tetragonal phase of CsSnI₃, CsSnI₂Cl, CsSnICl₂ and CsSnCl₃ increases and reaches its maximum value of 7.27, 8.13, 4.69 and 4.41 at 1.80, 0.73, 1.5 and 1.91 eV, respectively. Figure 9 (c) shows that $\epsilon_1(\omega)$ for the orthorhombic phase of CsSnI₃, CsSnI₂Cl, CsSnICl₂ and CsSnCl₃ increases and reaches its maximum value of 7.38, 5.89, 4.30 and 4.49 at 1.83, 1.67, 1.8 and 1.89 eV, respectively. Then at higher energy values, $\epsilon_1(\omega)$ becomes negative, which is explained by the fact that in this range, CsSnI_{3-x}Cl_x compounds will behave as a metal with high reflectivity of incident light. Based on the graphs and the given energy values at which the first peaks appear, it can be stated that these compounds exhibit good electro polarization properties in the visible range.

The imaginary parts of the dielectric function of CsSnI_{3-x}Cl_x for all x concentrations are shown in Figures 5(d), (e), (f) for α -, β -, γ - phases, respectively. It can be seen that the threshold values of $\epsilon_2(\omega)$ appear at 0.7 eV to 1.7 eV in general for the α -, β -, and γ - phases of CsSnI_{3-x}Cl_x (x = 0, 1, 2, 3), which is closely related to the band gap values. The first maximum peaks $\epsilon_2(\omega)$ for α -, β - and γ - phases of CsSnI_{3-x}Cl_x (x = 0, 1, 2, 3) occur at about 2.5 to 4 eV and then tends to 0 at high energies.

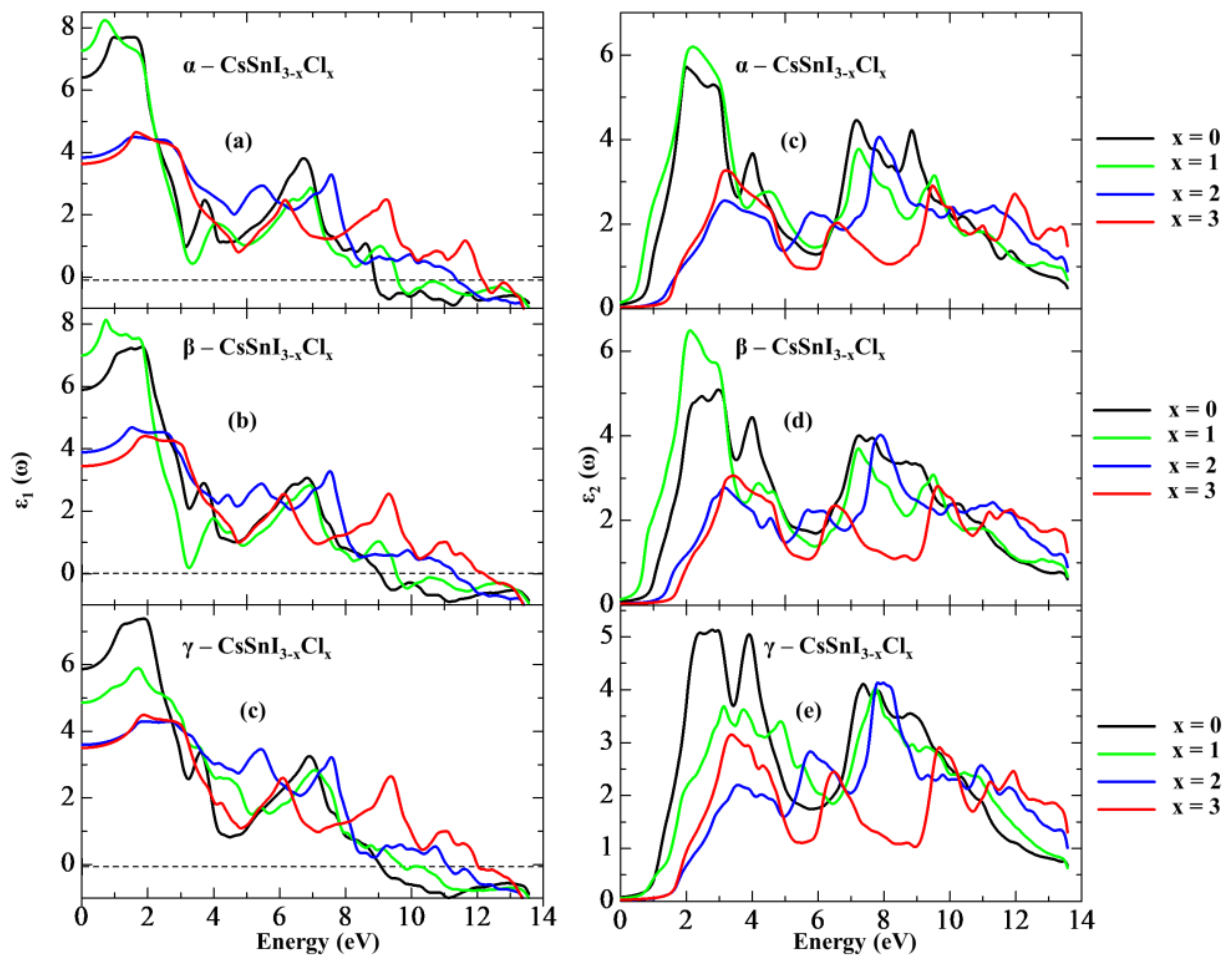


Figure 5. Calculated real part $\epsilon_1(\omega)$ and imaginary part $\epsilon_2(\omega)$ of dielectric permittivity as a function of energy using GGA - mBJ potential for α -, β - and γ - CsSnI_{3-x}Cl_x (x = 0, 1, 2, 3)

The refractive index $n(\omega)$ and reflectivity $R(\omega)$ were calculated for α -, β -, and γ -phases of CsSnI_{3-x}Cl_x (x = 0, 1, 2, 3) and are shown in Figure 6. The spectrum of $n(\omega)$ shown in Figure

6 (a), (b), (c) is very similar to the spectrum of $\varepsilon_1(\omega)$. The value of $n(\omega)$ describes the transparency and dispersion characteristics.

Table 3. Calculated and experimental band gap of α -, β - and γ - $\text{CsSnI}_{3-x}\text{Cl}_x$ ($x = 0, 1, 2, 3$) in eV.

System	Phases	This work		
		$\varepsilon_1(0)$	$n(0)$	$R(0)$
CsSnI3	α	6.41	2.53	0.188
	β	5.90	2.43	0.174
	γ	5.88	2.42	0.173
CsSnI ₂ Cl	α	7.27	2.70	0.211
	β	7.00	2.60	0.204
	γ	4.86	2.21	0.141
CsSnICl ₂	α	3.84	1.96	0.101
	β	3.89	1.97	0.107
	γ	3.60	1.90	0.095
CsSnCl ₃	α	3.64	1.91	0.097
	β	3.45	1.86	0.090
	γ	3.51	1.87	0.092

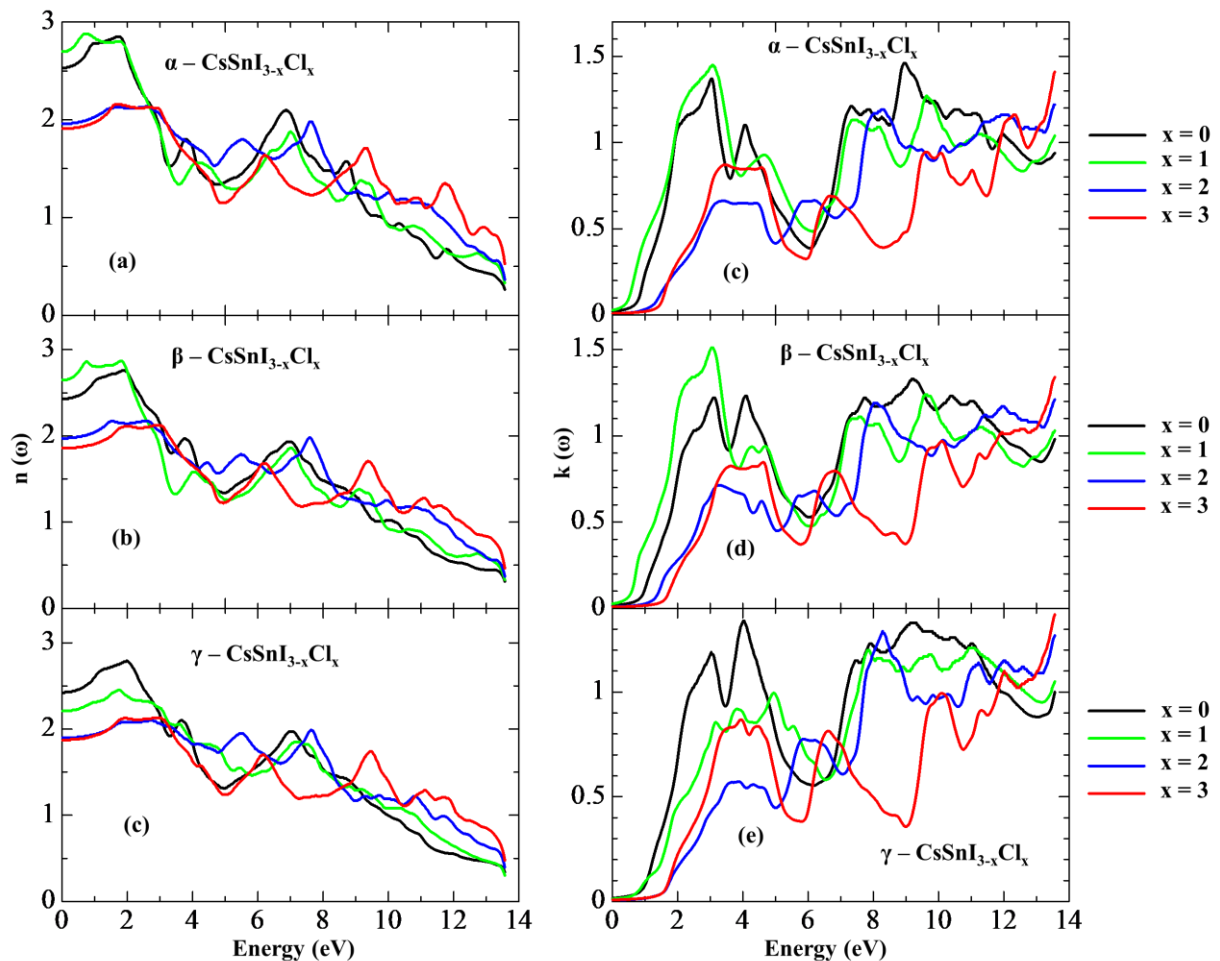


Figure 6. Calculated refractive index $n(\omega)$, коэффициент экстинкции $k(\omega)$ spectra of $\text{CsSnI}_{3-x}\text{Cl}_x$ perovskite using the GGA-mBJ potential

The calculated $n(0)$ for α -, β - and γ -phases of $\text{CsSnI}_{3-x}\text{Cl}_x$ ($x = 0, 1, 2, 3$) using the GGA-mBJ potential are presented in Table 3, whose value lies in the range of 1.8-2.7, which is desirable

for optoelectronic applications. For the α - and β -phases of $\text{CsSnI}_{3-x}\text{Cl}_x$, the highest value is achieved at $x=1$ than other concentrations, while for the γ -phase, the highest value is achieved at concentration $x = 0$. The first peaks in all systems are reached within 2 eV, then start to decrease and tend to 0 at high energies. This indicates that the refractive index of these perovskites is maximal at low photon energies.

The extinction coefficient $k(\omega)$ shown in Figure 6(d), (e), (f), demonstrates energy absorption and exhibits properties similar to those of $\varepsilon_2(\omega)$. The extinction coefficient (k) approaches a maximum value corresponding to the absorption maximum and then decreases as the absorption in the material decreases. The extinction coefficient for α -, β - and γ -phases of $\text{CsSnI}_{3-x}\text{Cl}_x$ ($x = 0, 1, 2, 3$) is shifted towards lower energies, with the first sharp peak appearing at an energy of about 3 eV and the second at an energy of about 9 eV, indicating better extinction coefficients (k) for these materials. However, high extinction coefficients (k) are observed for α -, β -phases of $\text{CsSnI}_{3-x}\text{Cl}_x$ at $x = 1$ compared to other compounds.

Fig. 7(a), (b), (c) shows the energy dependence of the absorption coefficient $\alpha(\omega)$ of α -, β -, and γ -phases of $\text{CsSnI}_{3-x}\text{Cl}_x$ ($x = 0, 1, 2, 3$). The absorption edge starts from energy 1 - 1.7 eV, which corresponds to the band gap of these materials. CsSnI_3 and CsSnI_2Cl have good absorption ability than CsSnICl_2 and CsSnCl_3 due to the smaller band gap in all investigated $\text{CsSnI}_{3-x}\text{Cl}_x$ phases. Due to the large band gap of α -, β - and γ -phases, CsSnCl_3 has weak light absorption in the visible region compared to other compounds, but their light absorption is significant in the UV region as well. It can be seen that the first characteristic peaks of the α -phases CsSnI_3 and CsSnI_2Cl appear in the vicinity of 3 eV, and for the α -phases CsSnICl_2 and CsSnCl_3 in the vicinity of 4.5 eV.

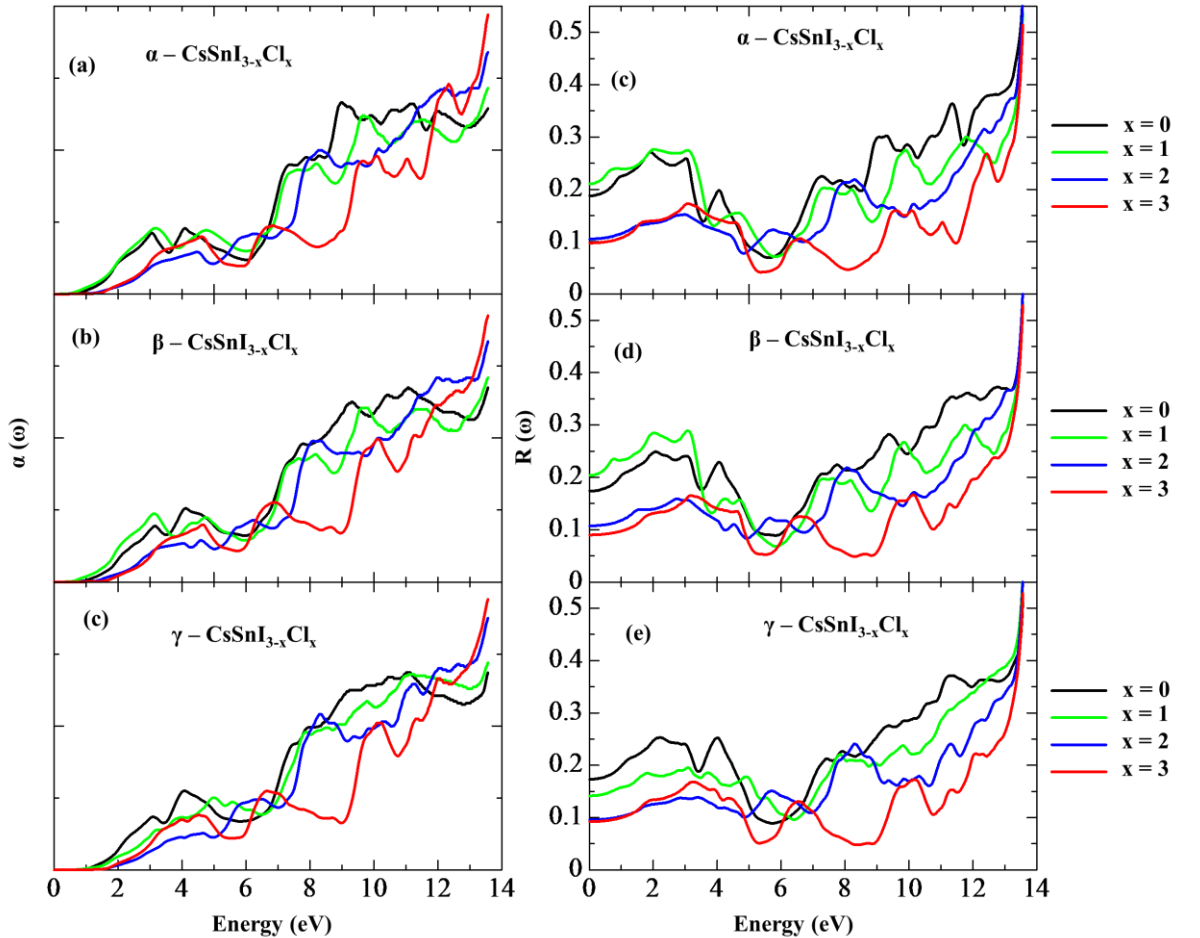


Figure 7. Calculated absorption coefficients spectra $\alpha(\omega)$ and reflectivity $R(\omega)$ of $\text{CsSnI}_{3-x}\text{Cl}_x$ perovskite using the GGA-mBJ potential

A similar trend is observed for the other $\text{CsSnI}_{3-x}\text{Cl}_x$ phases, but depending on the band gap, the appearance of the characteristic first peaks is observed at slightly higher energy values. In general, at $x=1$, an improvement in the absorption coefficient is observed, which is superior to the other studied compounds. Materials used in optoelectronic applications should have good extinction in the visible and near-UV range. Based on the results obtained such as absorption coefficient, $\alpha(\omega)$, it can be stated that $\text{CsSnI}_{3-x}\text{Cl}_x$ is a good material for optoelectronic applications.

The reflectivity $R(\omega)$ determining the nature of the surface of materials for optoelectronics and solar cells are presented in Figure 7(d), (e), (f) for α -, β - and γ - phases of $\text{CsSnI}_{3-x}\text{Cl}_x$ ($x = 0, 1, 2, 3$), respectively. The calculated values of $R(0)$ for the investigated systems are presented in Table 3. From the results obtained, it can be seen that the reflectivity is very low for all the studied perovskite compounds. However, in α - and β - phases, the reflectivity shows a maximum at $x = 1$ and a minimum at $x = 3$, in the optical range. In γ - phases of $\text{CsSnI}_{3-x}\text{Cl}_x$, the reflectivity shows a maximum at $x = 0$. $R(\omega)$ finds a first maximum peak in the vicinity from 4 eV and minimum values in the vicinity of 6 eV for all the studied systems, then starts to increase with increasing photon energies.

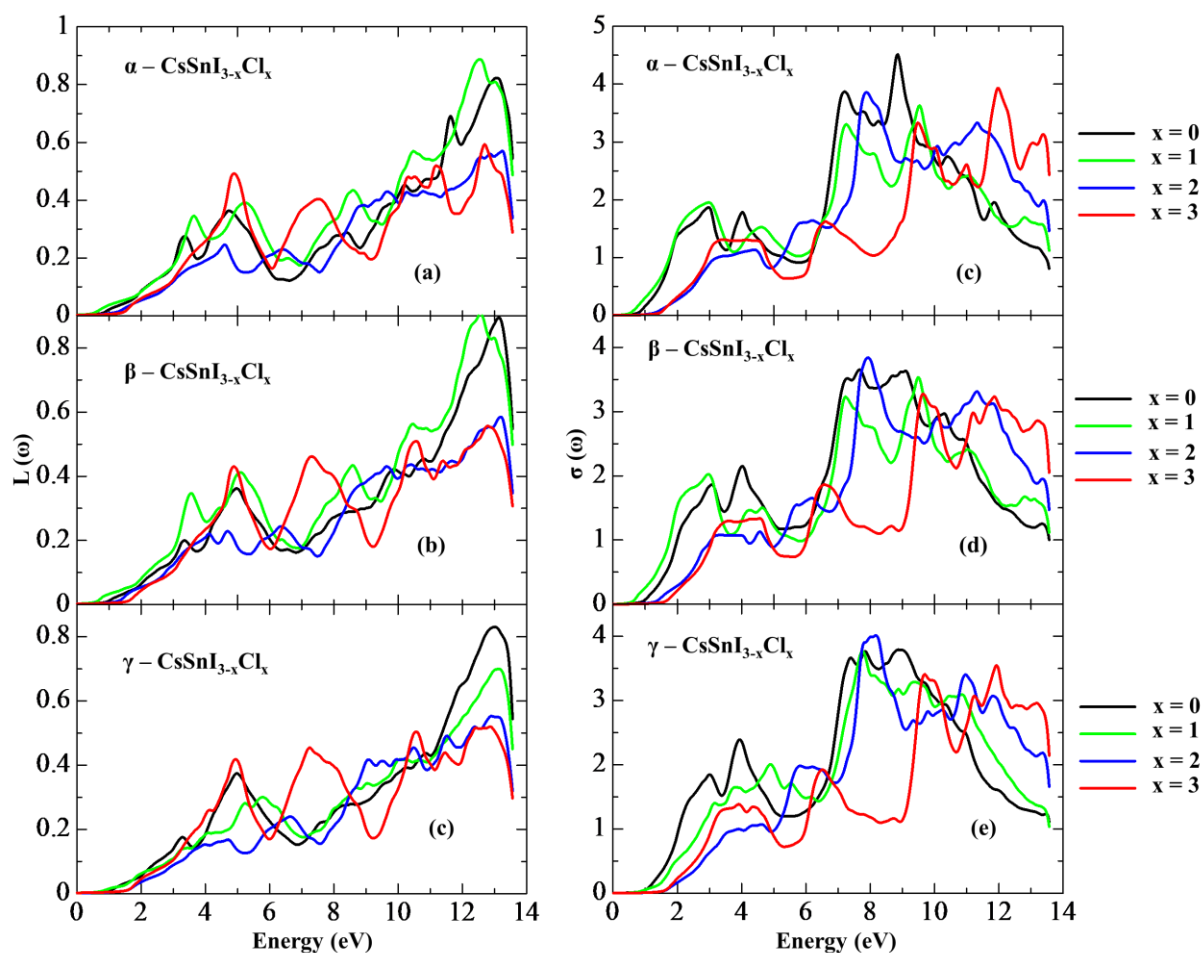


Figure 8. Calculated функция потерь энергии $L(\omega)$ и оптической проводимости $\sigma(\omega)$ of $\text{CsSnI}_{3-x}\text{Cl}_x$ perovskite using the GGA-mBJ potential

The electron energy loss function $L(\omega)$, which measures the energy loss during propagation inside the material, is shown in Figure 8 (a), (b), (c) for the α -, β -, and γ -phases of $\text{CsSnI}_{3-x}\text{Cl}_x$ ($x = 0, 1, 2, 3$), respectively. The peaks in the plots of the electron energy loss function for $\text{CsSnI}_{3-x}\text{Cl}_x$ characterize that the energy loss occurs when the incident photon energy is above the band gap of the material. $L(\omega)$ has a small value up to 10 eV and increases above it for all investigated systems.

The optical conductivity $\sigma(\omega)$ is another important parameter that determines the photovoltaic applications of materials. Figure 8 (d), (e), (f) show the calculated spectra of $\sigma(\omega)$ for α -, β - and γ -phases of $\text{CsSnI}_{3-x}\text{Cl}_x$ ($x = 0, 1, 2, 3$). It can be seen that $\sigma(\omega)$ has exactly the same variations as $\alpha(\omega)$, $k(\omega)$ and $\varepsilon_2(\omega)$, and indicates the conditioned absorption of the incoming energies. The larger absorption and photoconductivity in perovskite compounds based on α -, β -, and γ -phases of $\text{CsSnI}_{3-x}\text{Cl}_x$, observed respectively at $x=1$ and $x = 0$, may be due to the smaller magnitude of their band gap.

3.4. Elastic properties

Modeling of mechanical properties of perovskites of the α - $\text{CsSnI}_{3-x}\text{Cl}_x$ family, namely, determination of their elastic constants, allows us to obtain a detailed understanding of the material behavior under macroscopic pressure. From this point of view, in this work, first-principles calculations are carried out to obtain relaxed structures of crystals of the α - $\text{CsSnI}_{3-x}\text{Cl}_x$ family ($x = 0, 1, 2, 3$) under pressure in the range from 0 to 30 GPa, in which the external pressure induction increases in steps of 5 GPa. The obtained results will allow us to understand the nature of the investigated materials in terms of their natural response to pressure-like external perturbations.

Under the action of pressure, the structural parameters of the materials change markedly. The calculated lattice constant a of α - $\text{CsSnI}_{3-x}\text{Cl}_x$ ($x = 0, 1, 2, 3$) are summarized in Table 4 and plotted in Figure 9. The results obtained show that with increasing pressure the crystal constants of all compounds decrease.

Table 4. Calculated values of lattice constants a of α - $\text{CsSnI}_{3-x}\text{Cl}_x$ ($x = 0, 1, 2, 3$) within the GGA framework.

Pressure (GPa)	0	5	10	15	20	25	30
System\parameter	a (Å)						
CsSnI_3	6.259	5.853	5.643	5.498	5.39	5.302	5.227
CsSnI_2Cl	6.304	5.909	5.699	5.556	5.445	5.356	5.282
CsSnICl_2	6.291	5.902	5.693	5.548	5.437	5.347	5.27
CsSnCl_3	5.617	5.333	5.165	5.044	4.949	4.871	4.804

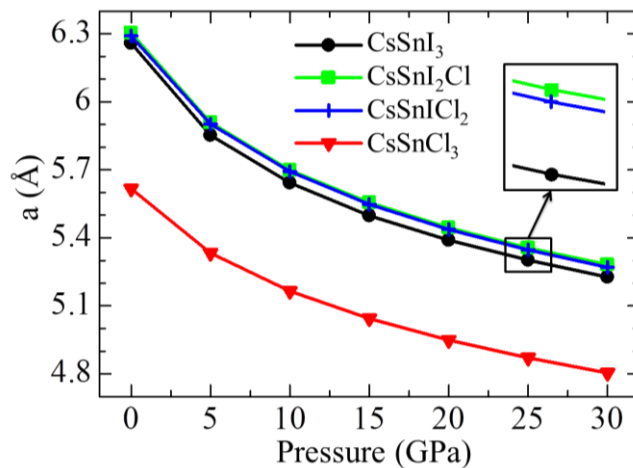


Figure 9. Calculated lattice constant a of α - $\text{CsSnI}_{3-x}\text{Cl}_x$ ($x = 0, 1, 2, 3$) as a function of pressure

The calculated pressure dependence of the relative volume change V/V_0 for α - $\text{CsSnI}_{3-x}\text{Cl}_x$ ($x = 0, 1, 2, 3$) is plotted in Figure 10, which is fitted to the Murnaghan's equation of state [69] expressed by:

$$V/V_0 = \left(1 + P \frac{B'}{B}\right)^{-\frac{1}{B'}}, \quad (9)$$

where V and V_0 are volumes at pressure P and ambient pressure, respectively, and B and B' are bulk modulus and its pressure derivative, respectively. With increasing pressure, the relative

volume of the lattice decreases. When moving from I to Cl, the relative volume of the systems under study increases.

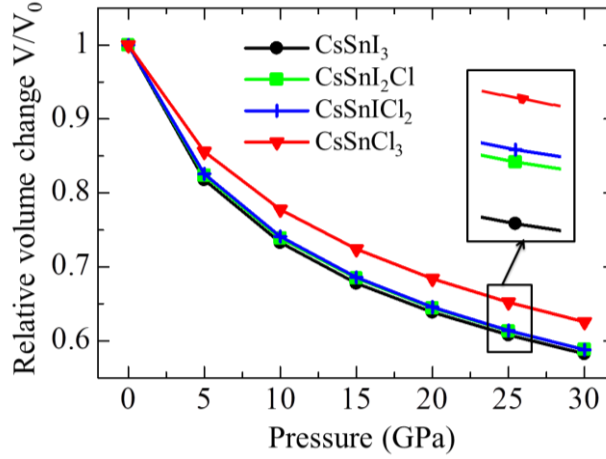


Figure 10. Calculated relative volume V/V_0 of α - $\text{CsSnI}_{3-x}\text{Cl}_x$ ($x = 0, 1, 2, 3$) as a function of pressure

The elasticity constant characterizes the stiffness of the crystal in response to external deformation, which can reflect the mechanical stability of the structure [70]. For this purpose, the elasticity coefficients C_{ij} describing the mechanical and dynamic behavior of the crystal are used. The cubic crystal system $\text{CsSnI}_{3-x}\text{Cl}_x$ has three necessary constants, C_{11} , C_{12} and C_{44} . For cubic symmetry, perovskite materials must satisfy the Born stability criteria: $C_{11} > 0$, $C_{44} > 0$, $C_{11} - C_{12} > 0$ and $C_{11} + 2C_{12} > 0$. The values we obtained satisfy the fundamental stability requirements [75], except for CsSnI_2Cl and CsSnICl_2 at pressures above 20 GPa. Knowing the elastic constants, we can calculate the values of bulk modulus (B) using Eq.:

$$B = \frac{C_{11} + 2C_{12}}{3}. \quad (10)$$

The elastic constants of the perovskite α - $\text{CsSnI}_{3-x}\text{Cl}_x$ family are calculated using the stretch-strain method [71] implemented in VASP, and the bulk moduli B are summarized in Table 5 and presented in Figure 11 as a function of pressure.

Coefficient C_{11} characterizes the shear pressure, which increases from 35.5 to 253.8, from 37.5 to 253.8, from 41.4 to 259.4, and from 47.9 to 244.7 for CsSnI_3 , CsSnI_2Cl , CsSnICl_2 , and CsSnCl_3 , respectively, with increasing pressure from 0 to 30 GPa. In turn, C_{12} details the lateral growth of the materials, which also increases from 5.01 to 21.5, from 5.17 to 6.73, from 5.98 to 13.9, and from 7.9 to 25.2 for CsSnI_3 , CsSnI_2Cl , CsSnICl_2 , and CsSnCl_3 , respectively, with increasing pressure. CsSnI_3 and CsSnCl_3 exhibit cubic stability up to 30 GPa as they satisfy the corresponding stability conditions. The compounds CsSnI_2Cl and CsSnICl_2 exhibit cubic stability up to 20 GPa, but beyond this pressure threshold, the elastic constant C_{44} becomes negative, resulting in loss of cubic stability.

Table 5. Pressure dependence of the elastic constants C_{ij} (all in GPa) and bulk moduli B for the α - $\text{CsSnI}_{3-x}\text{Cl}_x$ ($x = 0, 1, 2, 3$).

System	Pressure	C_{11}	C_{12}	C_{44}	B
CsSnI_3	0	35.50114	5.01589	5.92882	15.17764
	5	81.17576	8.37204	7.26883	32.63995
	10	117.8536	9.0661	8.19573	45.32861
	15	156.116	13.12337	9.03331	60.78759
	20	188.5391	14.69204	9.85631	72.64104
	25	222.2462	18.54959	10.7723	86.44844
	30	253.8087	21.58532	11.44541	98.99311
CsSnI_2Cl	0	37.58026	5.17644	5.89161	15.97771

	5	80.97833	5.09476	4.25839	30.38928
	10	119.374	4.75857	2.90674	42.96371
	15	155.4265	4.78352	1.38603	54.99783
	20	190.3706	5.43216	-0.18479	67.07832
	25	223.0629	6.14079	-1.79044	78.44816
	30	254.163	6.73404	-3.47802	89.21037
CsSnCl ₂	0	41.49006	5.98859	6.03352	17.82241
	5	86.05495	7.58443	4.41492	33.74127
	10	125.7027	8.8823	2.85454	47.82242
	15	162.9949	10.63699	1.12682	61.42296
	20	197.5641	11.91841	-0.76927	73.8003
	25	229.9778	13.44107	-2.45473	85.61997
CsSnCl ₃	0	47.93337	7.99036	7.67982	21.3047
	5	88.18753	10.92013	7.45618	36.67593
	10	122.7583	13.42084	6.81187	49.86665
	15	155.9491	16.28496	5.94841	62.83966
	20	186.3445	18.90914	5.2206	74.72093
	25	216.1941	22.26685	4.64435	86.90926
	30	244.7027	25.26311	3.6989	98.40963

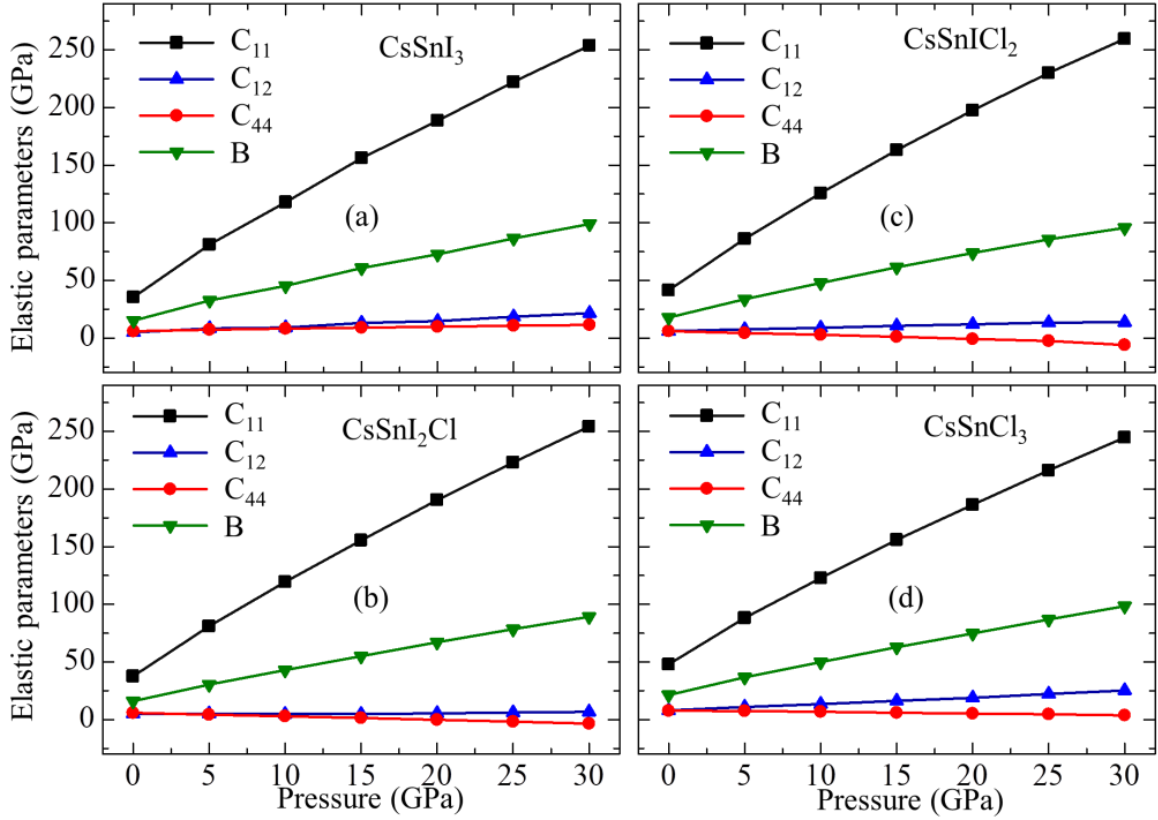


Figure 11. Calculated elastic constants C_{ij} and bulk moduli B for α -CsSnI_{3-x}Cl_x ($x = 0, 1, 2, 3$) as a function of pressure

Using these calculated elastic constants, sound velocities can be obtained. The mean sound velocity v_m is expressed [73] in terms of the longitudinal sound velocity v_l and the transverse one v_t as:

$$v_m = \left[\frac{1}{3} \left(\frac{2}{v_t^3} + \frac{1}{v_l^3} \right) \right]^{-1/3}, \quad (11)$$

in which v_l and v_t are calculated [74] by:

$$v_l = \sqrt{\frac{3B+4G}{3\rho}} \quad \text{and} \quad v_t = \sqrt{\frac{G}{\rho}}, \quad (12)$$

where

$$G = \frac{(G_V+G_R)}{2} \begin{cases} G_V = \frac{(C_{11}-C_{12}+3C_{44})}{5} \\ G_R = \frac{5(C_{11}-C_{12})C_{44}}{[4C_{44}+3(C_{11}-C_{12})]} \end{cases} .$$

Here: G is the isotropic shear modulus, G_V is the Voigt's shear modulus (an upper limit for G), and G_R is the Reuss's shear modulus (a lower limit for G).

The Debye temperature, which is sensitive to various physical parameters such as melting point, phonon heat capacity and elastic constants, can be calculated using Eq. [74]:

$$\theta_D = \frac{h}{k} \left(\frac{3n}{4\pi} \left(\frac{N_A \rho}{M} \right) \right)^{1/3} v_m, \quad (13)$$

where h and k are the Planck's and Boltzmann's constants, respectively. N_A is the Avogadro's number, ρ is the density, M is the molecular weight, and n denotes the number of atoms per formula unit (here five for α -CsSnI_{3-x}Cl_x).

Table 6. Calculated shear moduli, sound velocities and Debye temperatures for α -CsSnI_{3-x}Cl_x

System	P, GPa	G, GPa	v_t , m/s	v_l , m/s	v_m , m/s	θ_D , K
CsSnI ₃	0	8.750501	1429.506	2503.809	1588.557	140.5390
	5	14.80675	1681.55	3162.803	1878.963	177.7619
	10	19.54382	1828.867	3495.32	2045.809	200.7492
	15	23.9522	1947.117	3831.026	2182.152	219.7754
	20	27.97793	2042.693	4049.328	2290.312	235.2907
	25	31.98697	2130.877	4280.861	2391.072	249.7192
	30	35.60567	2200.648	4463.354	2470.712	261.7390
CsSn ₂ Cl	0	8.959554	1580.841	2790.822	1757.899	146.5787
	5	12.16749	1671.831	3272.227	1873.028	166.6186
	10	14.67662	1739.129	3589.812	1954.447	180.268
	15	16.62113	1781.535	3838.472	2006.457	189.8283
	20	18.28421	1812.824	4054.401	2045.14	197.4324
	25	19.64644	1833.258	4230.947	2070.851	203.2365
	30	20.74578	1844.944	4378.975	2086.247	207.6159
CsSnICl ₂	0	9.459279	1776.437	3186.441	1977.966	155.3741
	5	12.5939	1862.602	3731.025	2089.684	174.969
	10	14.84213	1915.584	4088.507	2156.446	187.1876
	15	16.50368	1943.285	4369.196	2192.81	195.3189
	20	17.68917	1951.794	4579.607	2206.142	200.5181
	25	18.84025	1964.49	4762.768	2223.078	205.4585
	30	17.67226	1861.672	4835.181	2111.187	197.9683
CsSnCl ₃	0	11.39221	1842.915	3298.48	2051.627	167.3162
	5	15.46876	1986.688	3823.692	2223.384	190.9796
	10	18.21849	2054.974	4145.997	2306.468	204.5602
	15	20.44157	2100.702	4410.195	2362.887	214.5912
	20	22.48657	2141.324	4620.622	2411.843	223.2418
	25	24.53656	2184.131	4822.611	2462.653	231.595
	30	26.06829	2204.984	4983.655	2488.659	237.3047

The calculated sound velocities v_m , v_t and v_l , shear modulus G and Debye temperature θ_D as a function of pressure, which are examples of the fundamental mechanical properties of α -

$\text{CsSnI}_{3-x}\text{Cl}_x$ to determine their hardness or stability, are summarized in Table 6 and are plotted in Figures 12, 13a, and 13b for sound velocities, shear moduli, and Debye temperatures, respectively. The v_m , v_t , v_l , G , and θ_D values for all systems increase with pressure.

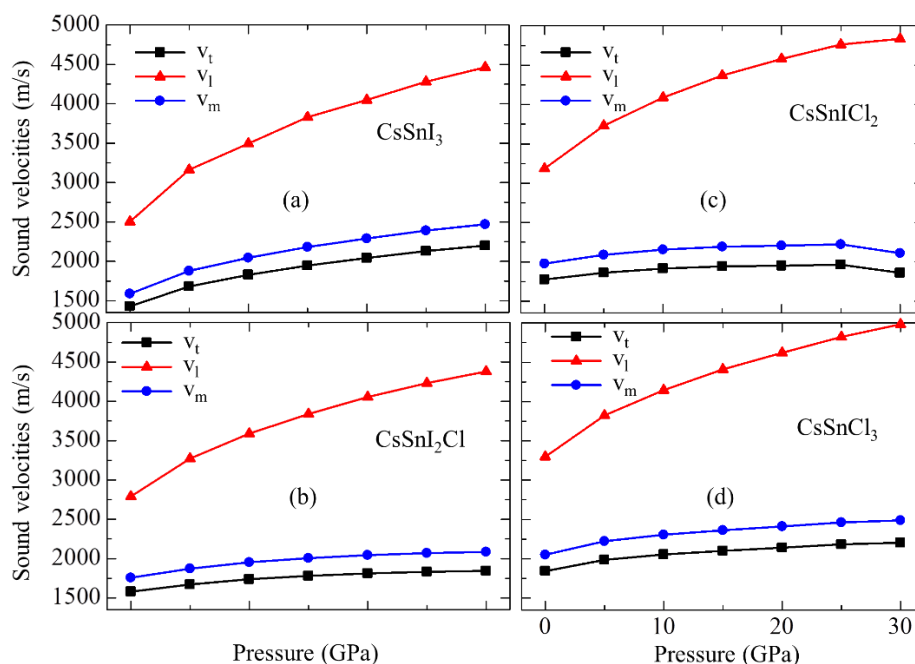


Figure 12. Calculated sound velocities for $\alpha\text{-CsSnX}_3$ ($X = \text{I, Br and Cl}$) as a function of pressure

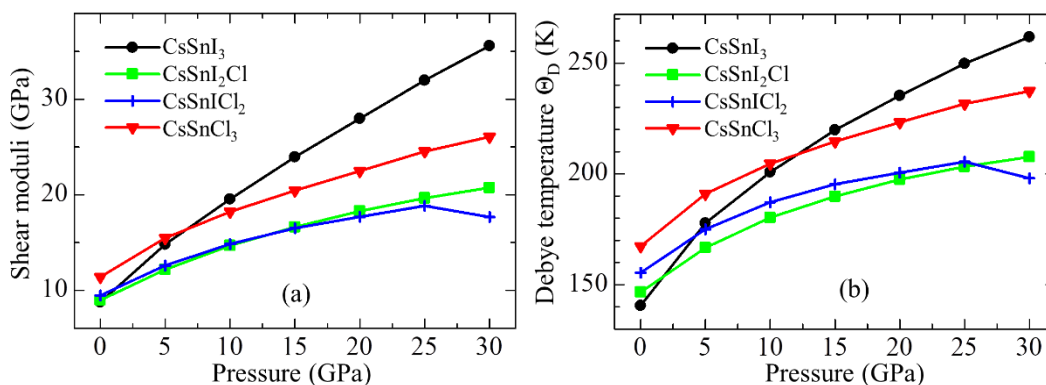


Figure 13. Calculated (a) shear moduli and (b) Debye temperatures for $\alpha\text{-CsSnI}_{3-x}\text{Cl}_x$ as a function of pressure

4. Conclusions

The structural, electronic, optical and elastic properties of compounds such as α -, β - and γ -phases $\text{CsSnI}_{3-x}\text{Cl}_x$ ($x = 0, 1, 2, 3$) were studied DFT using GGA, SCAN and HSE06. As a result, it is found that the position I(1) is energetically more favorable for Cl ions in CsSnI_3 . We find that the lattice constants of $\text{CsSnI}_{3-x}\text{Cl}_x$ decrease with decreasing the size of anions from I to Cl. It is found that the band gap of $\text{CsSnI}_{3-x}\text{Cl}_x$ at transition from CsSnI_3 to CsSnCl_3 first slightly decreases and then increases. This trend appears to be the same in all investigated $\text{CsSnI}_{3-x}\text{Cl}_x$ phases. The total and partial densities of states reflecting the semiconducting properties of the studied systems have been calculated and discussed. The obtained lattice parameters and band gap of the studied systems are in good agreement with experimental and other theoretical works. Optical properties such as complex dielectric function, absorption coefficient, reflectivity, refractive index, extinction coefficient, optical conductivity and energy loss function for pure and mixed cases are discussed. The low reflectivity, wide absorption range and high absorption coefficients of these compounds make them good candidates for various optoelectronic and photovoltaic applications.

The mechanical properties of α -CsSnI_{3-x}Cl_x have been investigated using the GGA approximation. The elastic constants C_{ij} for α -CsSnI_{3-x}Cl_x were calculated and their bulk moduli, shear moduli, sound velocities and Debye temperatures were discussed. The materials are found to be mechanically stable perovskites according to Born stability criteria and low bulk moduli. Thus, in general, perovskites of the CsSnI_{3-x}Cl_x family are good candidates for optical materials used in solar cells. The results obtained in this work provide a theoretical basis for the experimental study of mixed perovskites, allowing further investigation of other types of materials with suitable properties and finding potential applications in the semiconductor and optoelectronic industries.

Funding

The work was performed at the S.U. Umarov Physical-Technical Institute of the National Academy of Sciences of Tajikistan with the support of International Science and Technology Center (ISTC), project TJ-2726.

References

1. Liang, J., Liu, J., Jin, Z. (2017). All-inorganic halide perovskites for optoelectronics: progress and prospects. *Solar Rrl*, 1 (10), 1700086.
2. Tian, J., Xue, Q., Yao, Q., Li, N., Brabec, C. J., Yip, H. L. Inorganic halide perovskite solar cells: progress and challenges. *Advanced energy materials*, (2020), 10 (23), 2000183.
3. Green, M. A., Ho-Baillie, A., & Snaith, H. J. The emergence of perovskite solar cells. *Nature photonics*, (2014), 8 (7), 506-514.
4. Eperon, G. E., Paternò, G. M., Sutton, R. J., Zampetti, A., Haghighirad, A. A., Cacialli, F., Snaith, H. J. Inorganic caesium lead iodide perovskite solar cells. *Journal of Materials Chemistry A*, (2015), 3 (39), 19688-19695.
5. Afsari, M., Boochani, A., Hantezadeh, M. Electronic, optical and elastic properties of cubic perovskite CsPbI₃: Using first principles study. *Optik*, (2016), 127 (23), 11433-11443.
6. Shai, X. X., Li, D., Liu, S. S., Li, H., Wang, M. K. Advances and Developments in Perovskite Materials for Solar Cell Applications. *Acta Physico-Chimica Sinica*, (2016), 32(9), 2159-2170.
7. Kojima, A., Teshima, K., Shirai, Y., Miyasaka, T. Organometal halide perovskites as visible-light sensitizers for photovoltaic cells. *Journal of the american chemical society*, (2009), 131 (17), 6050-6051.
8. Lakhdar, N., Hima, A. Electron transport material effect on performance of perovskite solar cells based on CH₃NH₃GeI₃. *Optical Materials*, (2020), 99, 109517.
9. Heo, J. H., Im, S. H. CH₃NH₃PbBr₃-CH₃NH₃PbI₃ perovskite-perovskite tandem solar cells with exceeding 2.2 V open circuit voltage. *Advanced Materials*, (2016), 28(25), 5121-5125.
10. Wang, Y. C., Wang, D. Y., Jiang, Y. T., Chen, H. A., Chen, C. C., Ho, K. C., Chen, C. W. FeS₂ nanocrystal ink as a catalytic electrode for dye-sensitized solar cells. *Angewandte Chemie*, (2013), 125 (26), 6826-6830.
11. Rezig, B., Dahman, H., Kenzari, M. Iron pyrite FeS₂ for flexible solar cells. *Renewable Energy*, (1992), 2(2), 125-128.
12. Song, C., Wang, S., Dong, W., Fang, X., Shao, J., Zhu, J., Pan, X. Hydrothermal synthesis of iron pyrite (FeS₂) as efficient counter electrodes for dye-sensitized solar cells. *Solar Energy*, (2016), 133, 429-436.
13. Gloeckler, M., Sankin, I., Zhao, Z. CdTe solar cells at the threshold to 20% efficiency. *IEEE Journal of Photovoltaics*, (2013), 3 (4), 1389-1393.
14. Bosio, A., Pasini, S., Romeo, N. The history of photovoltaics with emphasis on CdTe solar cells and modules. *Coatings*, (2020), 10(4), 344.
15. Mufti, N., Amrillah, T., Taufiq, A., Diantoro, M., Nur, H. Review of CIGS-based solar cells manufacturing by structural engineering. *Solar energy*, (2020), 207, 1146-1157.
16. Kessler, F., Rudmann, D. Technological aspects of flexible CIGS solar cells and modules. *Solar energy*, (2004), 77 (6), 685-695.

17. Evarestov, R. A., Kotomin, E. A., Senocrate, A., Kremer, R. K., Maier, J. First-principles comparative study of perfect and defective CsPbX₃ (X= Br, I) crystals. *Physical Chemistry Chemical Physics*, (2020), 22 (7), 3914-3920.
18. Di Liberto, G., Fatale, O., Pacchioni, G. Role of surface termination and quantum size in α -CsPbX₃ (X= Cl, Br, I) 2D nanostructures for solar light harvesting. *Physical Chemistry Chemical Physics*, (2021), 23 (4), 3031-3040.
19. Abdulkareem, N. A., Sami, S. A., Elias, B. H. Structural, electronic and optical properties of cubic perovskite CsPbX₃ (X= Br, Cl and I). *Science Journal of University of Zakho*, (2020), 8 (1), 23-28.
20. Chen, L. C., Tien, C. H., Tseng, Z. L., Ruan, J. H. Enhanced efficiency of MAPbI₃ perovskite solar cells with FAPbX₃ perovskite quantum dots. *Nanomaterials*, (2019), 9 (1), 121.
21. Belous, A. G., Ishchenko, A. A., V'yunov, O. I., Torchyniuk, P. V. Preparation and Properties of Films of Organic-Inorganic Perovskites MAPbX₃ (MA= CH₃NH₃; X= Cl, Br, I) for Solar Cells: A Review. *Theoretical and Experimental Chemistry*, (2021), 56, 359-386.
22. Kenfack, A. K., Msimanga, M., Thantsha, N. M. Computational modelling and improvement of heterojunction perovskite solar cell based on CsPbI₃/MAPbX₃ (X= I_{1-x}Br_x). *Optik*, (2023), 289, 171288.
23. Lang, L., Yang, J. H., Liu, H. R., Xiang, H. J., Gong, X. G. First-principles study on the electronic and optical properties of cubic ABX₃ halide perovskites. *Physics Letters A*, (2014), 378 (3), 290-293.
24. Murtaza, G., Ahmad, I. First principle study of the structural and optoelectronic properties of cubic perovskites CsPbM₃ (M= Cl, Br, I). *Physica B: Condensed Matter*, (2011), 406(17), 3222-3229.
25. Geisz, J. F., France, R. M., Schulte, K. L., Steiner, M. A., Norman, A. G., Guthrey, H. L., Moriarty, T. Six-junction III–V solar cells with 47.1% conversion efficiency under 143 Suns concentration. *Nature energy*, (2020), 5 (4), 326-335.
26. NREL, Best Research-Cell Efficiencies Chart (nrel.gov), (accessed: October 2023).
27. Kim, M., Jeong, J., Lu, H., Lee, T. K., Eickemeyer, F. T., Liu, Y., Kim, D. S. Conformal quantum dot–SnO₂ layers as electron transporters for efficient perovskite solar cells. *Science*, (2022), 375 (6578), 302-306.
28. Berhe, T. A., Su, W. N., Chen, C. H., Pan, C. J., Cheng, J. H., Chen, H. M., Hwang, B. J. Organometal halide perovskite solar cells: degradation and stability. *Energy & Environmental Science*, (2016), 9(2), 323-356.
29. Han, Q., Bae, S. H., Sun, P., Hsieh, Y. T., Yang, Y., Rim, Y. S., Yang, Y. Single crystal formamidinium lead iodide (FAPbI₃): insight into the structural, optical, and electrical properties. *Advanced Materials*, (2016), 28(11), 2253-2258.
30. Filip, M. R., Giustino, F. Computational screening of homovalent lead substitution in organic–inorganic halide perovskites. *The Journal of Physical Chemistry C*, (2016), 120 (1), 166-173.
31. Krishnamoorthy, T., Ding, H., Yan, C., Leong, W. L., Baikie, T., Zhang, Z., Mhaisalkar, S. G. Lead-free germanium iodide perovskite materials for photovoltaic applications. *Journal of Materials Chemistry A*, (2015), 3 (47), 23829-23832.
32. Oku, T., Ohishi, Y., Suzuki, A. Effects of antimony addition to perovskite-type CH₃NH₃PbI₃ photovoltaic devices. *Chemistry Letters*, (2016), 45 (2), 134-136.
33. Travis, W., Glover, E. N. K., Bronstein, H., Scanlon, D. O., Palgrave, R. G. On the application of the tolerance factor to inorganic and hybrid halide perovskites: a revised system. *Chemical science*, (2016), 7(7), 4548-4556.
34. Zuo, F., Williams, S. T., Liang, P. W., Chueh, C. C., Liao, C. Y., Jen, A. K. Y. Binary-metal perovskites toward high-performance planar-heterojunction hybrid solar cells. *Advanced Materials*, (2014), 26(37), 6454-6460.
35. Giustino, F., Snaith, H. J. Toward lead-free perovskite solar cells. *ACS Energy Letters*, (2016), 1 (6), 1233-1240.

36. Boix, P. P., Agarwala, S., Koh, T. M., Mathews, N., Mhaisalkar, S. G. Perovskite solar cells: beyond methylammonium lead iodide. *The journal of physical chemistry letters*, (2015), 6(5), 898-907.
37. Chakraborty, S., Xie, W., Mathews, N., Sherburne, M., Ahuja, R., Asta, M., Mhaisalkar, S. G. Rational design: A high-throughput computational screening and experimental validation methodology for lead-free and emergent hybrid perovskites. *ACS Energy Letters*, (2017), 2(4), 837-845.
38. Kagan, C. R., Mitzi, D. B., Dimitrakopoulos, C. D. Organic-inorganic hybrid materials as semiconducting channels in thin-film field-effect transistors. *Science*, (1999), 286 (5441), 945-947.
39. Stoumpos, C. C., Kanatzidis, M. G. The renaissance of halide perovskites and their evolution as emerging semiconductors. *Accounts of chemical research*, (2015), 48(10), 2791-2802.
40. Stoumpos, C. C., Malliakas, C. D., Kanatzidis, M. G. Semiconducting tin and lead iodide perovskites with organic cations: phase transitions, high mobilities, and near-infrared photoluminescent properties. *Inorganic chemistry*, (2013), 52(15), 9019-9038.
41. Kresse, G., Furthmüller, J. Efficiency of ab-initio total energy calculations for metals and semiconductors using a plane-wave basis set. *Computational materials science*, (1996), 6(1), 15-50.
42. Perdew, J. P., Burke, K., Wang, Y. Generalized gradient approximation for the exchange-correlation hole of a many-electron system. *Physical review B*, (1996), 54(23), 16533.
43. Bartók, A. P., & Yates, J. R. Regularized SCAN functional. *The Journal of chemical physics*, (2019), 150(16), 161101.
44. Deák, P., Aradi, B., Frauenheim, T., Janzén, E., Gali, A. Accurate defect levels obtained from the HSE06 range-separated hybrid functional. *Physical Review B*, (2010), 81 (15), 153203.
45. Yamada, K., Funabiki, S., Horimoto, H., Matsui, T., Okuda, T., Ichiba, S. Structural phase transitions of the polymorphs of CsSnI₃ by means of rietveld analysis of the X-ray diffraction. *Chemistry Letters*, (1991), 20(5), 801-804.
46. Kashikar, R., Khamari, B., Nanda, B. R. K. Second-neighbor electron hopping and pressure induced topological quantum phase transition in insulating cubic perovskites. *Physical Review Materials*, (2018), 2(12), 124204.
47. Voloshinovskii, A. S., Myagkota, S. V., Pidzyrailo, N. S., Tokarivskii, M. V. Luminescence and structural transformations of CsSnCl₃ crystals. *Journal of Applied Spectroscopy*, (1994), 60(3-4), 226-228.
48. Chen, Z., Wang, J. J., Ren, Y., Yu, C., Shum, K. Schottky solar cells based on CsSnI₃ thin-films. *Applied physics letters*, (2012), 101 (9).
49. Jurow, M. J., Morgenstern, T., Eisler, C., Kang, J., Penzo, E., Do, M., Liu, Y. Manipulating the transition dipole moment of CsPbBr₃ perovskite nanocrystals for superior optical properties. *Nano letters*, (2019), 19 (4), 2489-2496.
50. Kamat, P. V., Bisquert, J., Buriak, J. Lead-free perovskite solar cells. *ACS Energy Letters*, (2017), 2 (4), 904-905.
51. Kohn, W., Becke, A. D., Parr, R. G. Density functional theory of electronic structure. *The journal of physical chemistry*, (1996), 100 (31), 12974-12980.
52. Yamada, K., Kawaguchi, H., Matsui, T., Okuda, T., Ichiba, S. Structural Phase Transition and Electrical Conductivity of the Perovskite CH₃NH₃Sn_{1-x}Pb_xBr₃ and CsSnBr₃. *Bulletin of the Chemical Society of Japan*, (1990), 63 (9), 2521-2525.
53. Yuan, Y., Xu, R., Xu, H. T., Hong, F., Xu, F., Wang, L. J. Nature of the band gap of halide perovskites ABX₃ (A= CH₃NH₃, Cs; B= Sn, Pb; X= Cl, Br, I): First-principles calculations. *Chinese Physics B*, (2015), 24 (11), 116302.
54. Lang, L., Yang, J. H., Liu, H. R., Xiang, H. J., Gong, X. G. First-principles study on the electronic and optical properties of cubic ABX₃ halide perovskites. *Physics Letters A*, (2014), 378(3), 290-293.

55. Balasubramanian, K. Relativity and chemical bonding. *The Journal of Physical Chemistry*, (1989), 93 (18), 6585-6596.
56. Yamada, K., Kuranaga, Y., Ueda, K., Goto, S., Okuda, T., Furukawa, Y. Phase transition and electric conductivity of ASnCl_3 (A= Cs and CH_3NH_3). *Bulletin of the Chemical Society of Japan*, (1998), 71 (1), 127-134.
57. Wu, Z., Cohen, R. E. More accurate generalized gradient approximation for solids. *Physical Review B*, (2006), 73 (23), 235116.
58. Koller, D., Tran, F., Blaha, P. Improving the modified Becke-Johnson exchange potential. *Physical Review B*, (2012), 85 (15), 155109.
59. Blaha, P., Schwarz, K., Madsen, G. K. H., Kvasnicka, D., Luitz, J. WIEN2k, An Augmented Plane Wave Plus Local Orbitals Program for Calculating Crystal Properties (Vienna University of Technology, Austria, 2001). Google Scholar There is no corresponding record for this reference (2002).
60. Goldschmidt, V. M. Die gesetze der krystallochemie. *Naturwissenschaften*, (1926), 14(21), 477-485.
61. Li, C., Lu, X., Ding, W., Feng, L., Gao, Y., Guo, Z. Formability of abx_3 ($x = \text{f, cl, br, i}$) halide perovskites. *Acta Crystallographica Section B: Structural Science*, (2008), 64(6), 702-707.
62. Stojiljkovic, M. Linear regression in python. *Real Python*. <https://realpython.com/linear-regression-in-python/>. Accessed, (2021), 8.
63. Polman, A., Knight, M., Garnett, E. C., Ehrler, B., Sinke, W. C. Photovoltaic materials: Present efficiencies and future challenges. *Science*, (2016), 352 (6283), aad4424.
64. Shockley, W., Queisser, H. J. Detailed balance limit of efficiency of p-n junction solar cells. *Journal of applied physics*, (1961), 32 (3), 510-519.
65. Burkhonzoda, A. DFT Study on the Electronic Structure and Optical Properties of Orthorhombic Perovskite CsPbBr_3 Doped with I and Cl. *Biointerface Research in Applied Chemistry*, (2023), 13(6), 516
66. Li, W., Zhu, S., Zhao, Y., Qiu, Y. Structure, electronic and optical properties of $\text{Cs}_2\text{Ti}(\text{Br}_{1-x}\text{Y}_x)_6$ (Y= Cl, I; $x = 0, 0.25, 0.5, 0.75, 1$) perovskites: the first principles investigations. *Journal of Solid State Chemistry*, (2020), 284, 121213.
67. Burkhonzoda, A. S., Nematov, D. D., Khodzkhonov, I. T., Bobosheirov, D. I. Optical properties of nanocrystals of the $\text{TiO}_2\text{-xN}_x$ system. *SCI-ARTICLE. RU*, (2021), 92, 176-187.
68. Aktary, M., Kamruzzaman, M., Afrose, R. Pressure-dependent comparative study of the mechanical, electronic, and optical properties of CsPbX_3 (X= Cl, Br, I): a DFT study for optoelectronic applications. *Materials Advances*, (2023), 4 (19), 4494-4508.
69. Murnaghan, F. D. The compressibility of media under extreme pressures. *Proceedings of the National Academy of Sciences*, (1944), 30 (9), 244-247.
70. Tennakoon, S., Peng, Y., Mookherjee, M., Speziale, S., Manthilake, G., Besara, T., Rivera, F. Single crystal elasticity of natural topaz at high-temperatures. *Scientific reports*, (2018), 8 (1), 1372.
71. Nielsen, O. H., Martin, R. M. First-principles calculation of stress. *Physical Review Letters*, (1983), 50 (9), 697.
72. Maulud, D., Abdulazeez, A. M. A review on linear regression comprehensive in machine learning. *Journal of Applied Science and Technology Trends*, (2020), 1 (4), 140-147.
73. Poirier, J. P., Michael Brown, J. Introduction to the Physics of the Earth's Deep Interior. *Phys. Today*, (1992), 45, 66-67.
74. Anderson, O. L. A simplified method for calculating the Debye temperature from elastic constants. *Journal of Physics and Chemistry of Solids*, (1963), 24 (7), 909-917.
75. Mouhat, F., Coudert, F. X. Necessary and sufficient elastic stability conditions in various crystal systems. *Physical review B*, (2014), 90(22), 224104.